LA-UR-24-30540

Approved for public release; distribution is unlimited.

Title:	Key Degradation Products in Nitroplasticizer Thermal Aging
Author(s):	Chen, Kitmin Edgar, Alexander Steven Kress, Joel David Yang, Dali
Intended for:	Report
Issued:	2024-10-01

Key Degradation Products in Nitroplasticizer Thermal Aging

Kitmin Chen†, Alex Edgar†, Joel Kress‡, and Dali Yang (PI)†

†MST-7: Engineered Materials, Material Sciences and Technology Division, and ‡T-1: Physics and Chemistry of Materials, Theoretical Division, Los Alamos National Laboratory, Los Alamos, NM 87545, United States

Abstract

Upon thermal aging, nitroplasticizer (NP) can thermally degrade and release numerous degradation products depending on aging conditions. In this report, we summarize our recent findings, a library of key degradation products in the NP thermal aging is provided. The library contains 25 identified species with their corresponding MS/MS spectrum and intensity profiles, which are derived from our 44-month thermal aging experiment of NP conducted in air, nitrogen, and water at room temperature (RT), 38, 45, 55, and 64°C. To provide a comprehensive yet simplified overview of NP degradation, we summarized the proposed mechanisms of HONO elimination and decomposition, acid generation, PBNA nitrosation and nitration, acid-catalyzed hydrolyses of NP and polynitrated PBNAs, as well as the formation of NP degradants. As the last part of a series of publications and reports on the investigation of NP degradation mechanisms, this work further unfolds complex chemistry that occurs in the entire aging process of NP.

1. Introduction

In energetic material formulations, nitroplasticizer (NP), composed of bis(2,2-dinitropropyl) acetal and formal (BDNPA/F, 50/50 eutectic mixture, **Figure 1A**), is commonly used for reducing shock sensitivity and improving mechanical processing of highly explosive composites[1-4]. As the initial step of NP degradation, as shown in **reaction (1)** of **Figure 1B**, the elimination of HONO is achieved by intramolecular hydrogen transfer to the nearby NO_2 group[5, 6]. HONO can be decomposed in several paths, as highlighted in **reactions (2) to (4)**, producing small molecules, such as HNO_3, N_2O, NO, NO_2, and water. Among them, the presence of gaseous products N_2O and NO have been verified by the Constituent Aging Study (CAS)[7] and the generation of water has been verified[8] in addition to a trace amount of water originally present in NP[9, 10]. Due to hydrophobic nature of NP, the generated water and acidic species accumulate in isolated water droplets where the acidity can be very high and possibly promotes the formation of nitrosonium (NO^+) and nitronium (NO_2^+) ions[11], as shown in **reactions (5)** and **(6)** of **Figure 1C**. Continuing aging results in increased acidity, the deterioration of NP and nearby polymeric materials will inevitably occur[5, 6, 12-16]. Although 0.1 wt.% of N-phenyl-2-naphthylamine (PBNA, **Figure 1A**) was added more than 55 years ago after the production of NP in order to extend the shelf life[1, 3], little was reported about the effective scavenging property of PBNA and about the full picture of NP degradation mechanisms upon heating.

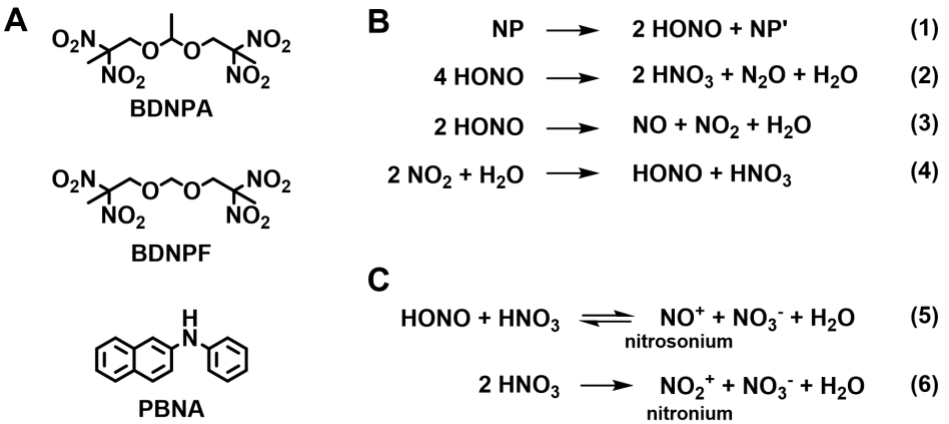

Figure 1. (A) Main components in NP. (B) NP degradation initiated from HONO elimination in reaction (1) and progressed into HONO decomposition in reactions (2) to (4), forming isolated highly acidic water droplets, which facilitates (C) the production of nitrosonium and nitronium ions in reaction (5) and (6).

In the early 2000s, Rindone et al. isolated the impurities associated with the ter Meer process of NP production (**Figure 2**), including 2-chloro-2,8,8-trinitro-4,6-dioxanonane (**I**), 2-chloro-5-methyl-2,8,8-trinitro-4,6-dioxanonane (**II**), 2,2,10,10-tetranitro-4,6,8-trioxaundecane (**III**), 5-methyl-2,2,10,10-tetranitro-4,6,8-trioxaundecane (**IV**), 2,6,-dimethyl-4-[2,2-dinitropropoxy]-1,3-dioxane (**V**), and 2,2-dinitropropyl acetate (**VI**). Among them, compound V was proposed as a probable cause of acid generation and accelerated aging of NP[17]. However, based on the kinetic compensation analysis of various product gases (e.g., N_2, NO, N_2O, CO, and CO_2) conducted in CAS, the degradation of NP was revealed being much more complex and could occur even under mild conditions (38-64°C)[7]. To understand what degradation species are being generated, how various species interact, and their cascaded effects, a 44-month long aging experiment was conducted at five temperatures (RT, 38, 45, 55, and 64°C) and three environments (with air, nitrogen, and added water above the NP matrix)[8, 18, 19]. The aged samples were analyzed using liquid chromatography tandem quadrupole time-of-flight mass spectrometry (LC-QTOF-MS) and ion chromatography (IC)[20-28]. Total of 25 key degradants were identified, along with 21 separate species not fully identified. Herein, we summarize these findings as a library of MS/MS information and their intensity or concentration profiles as a function of time.

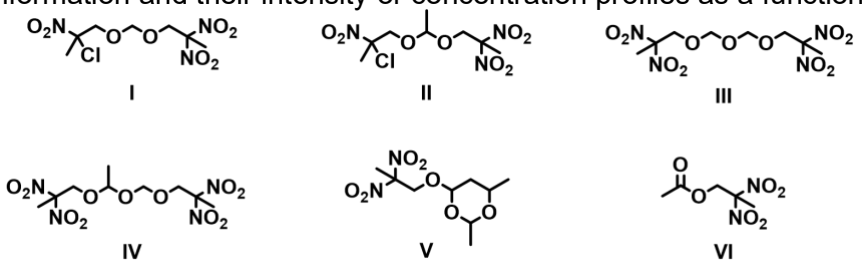

Figure 2. Isolated impurities proposed in the ter Meer synthesis of NP.

2. Experimental Section

In the thermal aging experiment, baseline NP samples, which had been stored at ambient conditions for more than 55 years, were artificially aged from 0 to 44 months RT, 38, 45, 55, and 64°C and sealed in air (A), nitrogen (N), or in contact with deionized water (W)[8, 18, 19]. The water-aged samples provide an additional sampling layer, referred to as the top aqueous layer (WW). The appearances of A samples and W samples are shown in **Figures 3**, respectively. The aging conditions change the color of NP samples significantly. The color change in the A samples is similar to that in the N samples. For the wet samples, while the color of W samples (at the bottom of vials) becomes lighter, the color of the WW samples gets darker, suggesting the significant degradation as the aging time and temperature increase.

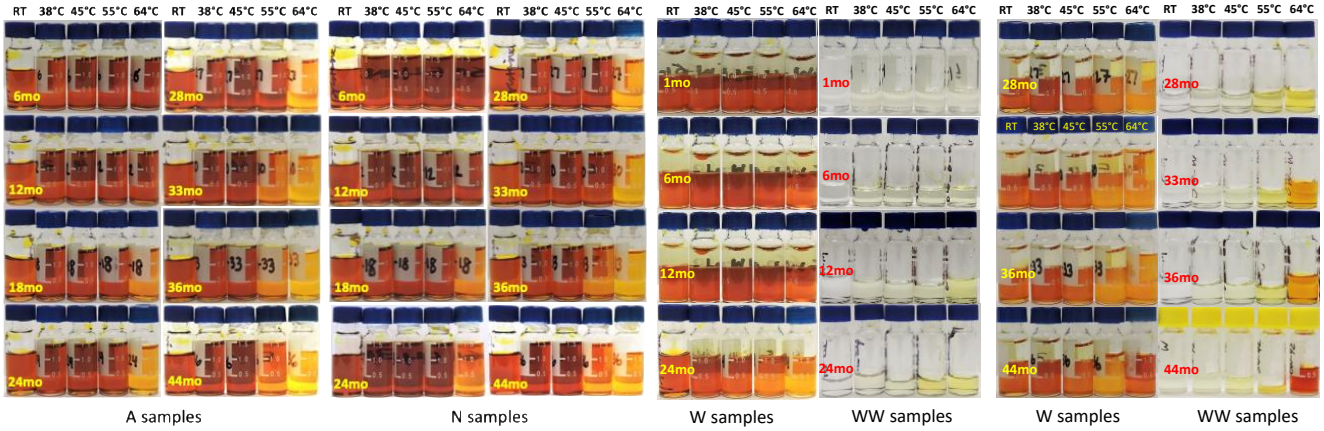

Figure 3. Appearances of A samples (left) and W and WW samples (right) aged at different times and temperatures.

All aged samples were stored under refrigeration (< 6°C) for over two years prior to the present study. The concentration profiles of acidic anions were obtained from IC analysis of the A, W, and WW samples. The MS/MS (fragment ion) spectra (with collision energy indicated by CID in V) and the intensity profiles

of A, N, and W samples were obtained from the LC-QTOF-MS analysis. Both the intensity and the concentration profiles were normalized individually using their maximum values, which are displayed on the top of each plot as 100%. Therefore, the work performed here does not provide quantitative assessment of the true concentration in any species but does provide accuracy necessary for qualitative comparisons. Further details on the methodology, analysis, and interpretation are documented in various publications[20-24, 26] and internal reports[25, 27, 28].

3. Results and Discussion

3.1 Acid Generation

As depicted in the IC spectrum of **Figure 4** and the acidic anion concentration profiles in **Figures 5 to 8**, The anion detection of nitrite (NO_2^-), nitrate (NO_3^-), acetate/formate ($RCOO^-$/$HCOO^-$), and oxalate ($C_2O_4^{2-}$) provides crucial evidence to HONO elimination in NP and the subsequent acid-catalyzed hydrolysis in NP and PBNA-associated products. The aqueous layer in the water-aged NP shows an extractive property towards water-soluble acids, which reduces the acidity in the NP phase, which in turn, may retard acid-catalyzed hydrolysis of NP at mild temperatures (<45°C)[22]. However, at elevated temperatures (≥55°C), assimilation between the aqueous and NP phases would rather promote a stronger hydrolytic effect after ~12 months of aging.

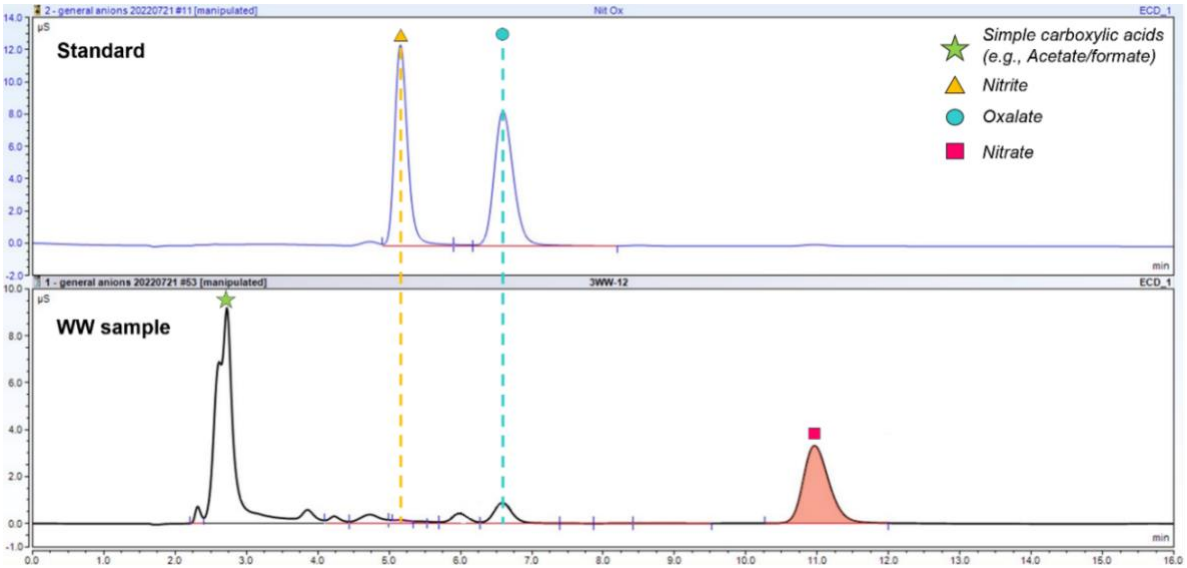

Figure 4. Example IC spectrum of acidic anions in the 12-month-aged WW sample at 38°C (bottom) and comparison to the reference standard of nitrite and oxalate anions (top): acetate/formate (green star), nitrite (yellow triangle), oxalate (teal circle), and nitrate (pink square). The absence of HONO detection in the WW sample at 38°C due to its poor solubility in the aqueous layer and potential conversion of HONO into HNO_3.

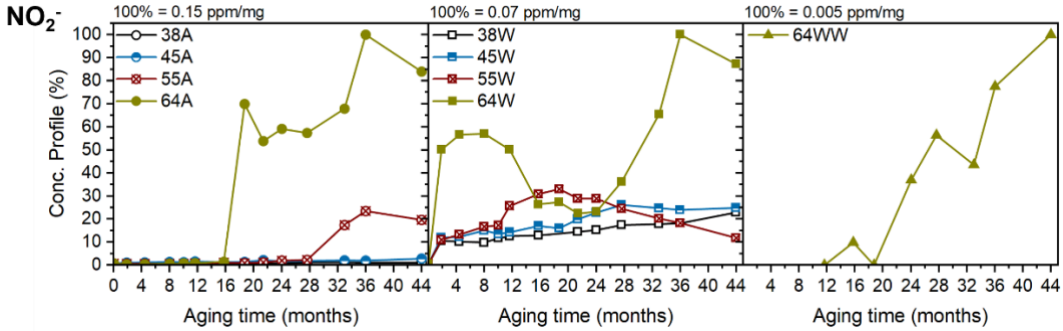

Figure 5. Concentration profile of nitrite anion (NO_2^-) in the A, W, and WW samples. At 64°C, the assimilation between NP and aqueous phases may allow for retention of HONO and thus detected in the WW samples.

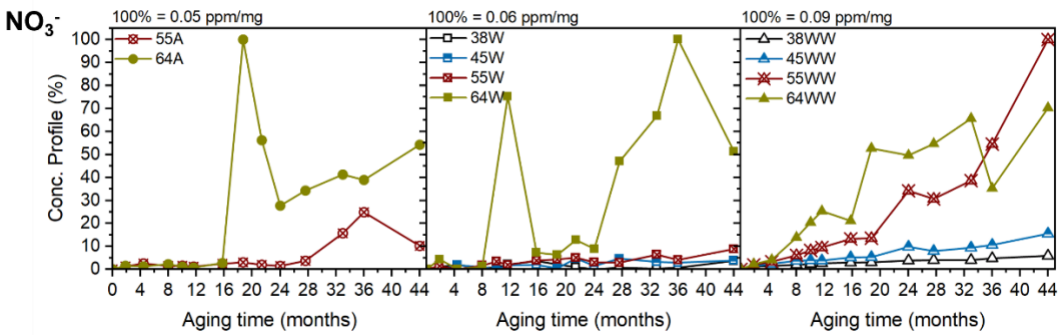

Figure 6. Concentration profile of nitrate anion (NO_3^-) in the A, W, and WW samples.

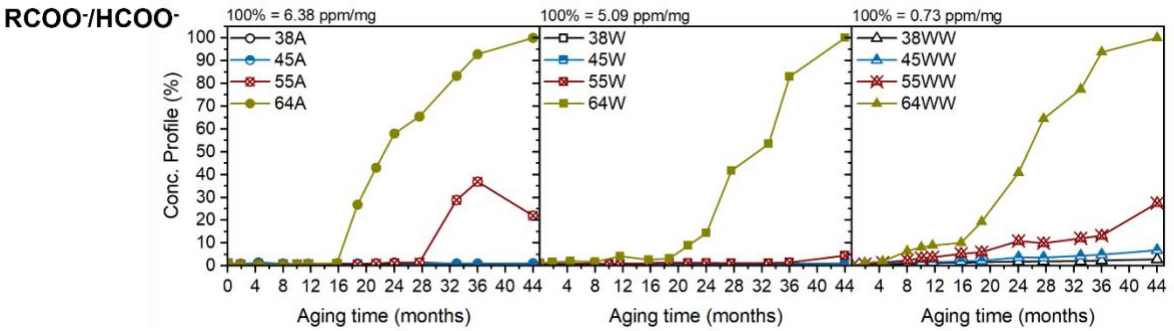

Figure 7. Concentration profile of acetate/formate anion ($RCOO^-/HCOO^-$) in the A, W, and WW samples.

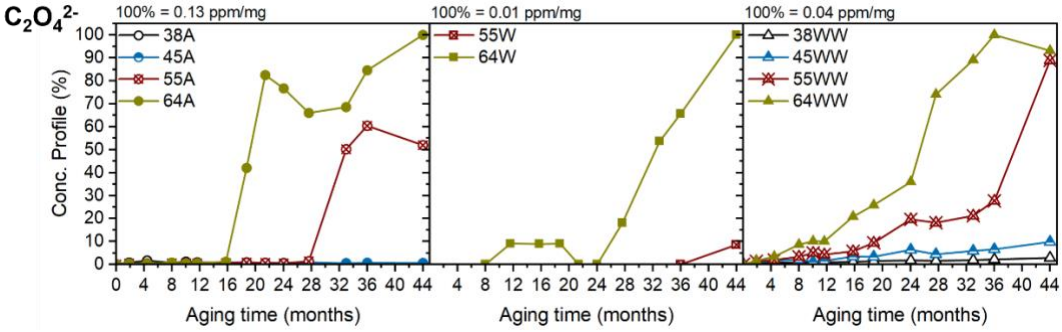

Figure 8. Concentration profile of oxalate anion ($C_2O_4^{2-}$) in the A, W, and WW samples.

3.2 PBNA Nitrosation in Early-stage and PBNA Nitration in Intermediate-stage Aging

The scavenging mechanism of PBNA (**Figure 9**) mainly starts with nitrosation and proceeds toward nitration. In nitrosation, the strong acid HNO_3 is utilized as a catalyst[29, 30] and thus the formation of nitroso-PBNA (**Figure 10**) from PBNA and NO^+ ion only consumes HONO, whereas HNO_3 is regenerated, as shown in **Reaction (7)** of **Scheme 1**. Likewise, other residual strong acids (e.g., HCl, H_2SO_4, etc.) may also promote nitrosation. As a result, a large abundance of nitroso-PBNA was detected in the early stage of NP aging[31], demonstrating its dominance over the nitration pathway. Assisted by the NO_2 radicals, nitroso-PBNA can be oxidized into mononitro-PBNA (**Reaction (8)** of **Scheme 1**). Additionally, various forms of polynitro compounds were generated through the sequential nitration pathway[21] by reacting with either NO_2 or NO_2^+ (**Reaction (9)** of **Scheme 1**), including mononitro-PBNA (**Figure 11**) and its isomer (**Figure 12**), dinitro-PBNA (**Figure 13**) and its isomer (**Figure 14**), trinitro-PBNA (**Figure 15**), tetranitro-PBNA (**Figure 16**), and pentanitro-PBNA (**Figure 17**). The isomeric species, as shown in **Figures 12** and **14**, share the same exact mass and similar concentration profiles to those in **Figures 11** and **13**, respectively, but with different fragmentation behavior. Besides mononitro-PBNA in **Figure 11**, which was verified using reference standard[23], the position of NO or NO_2 substitution in other PBNA species cannot be conclusively determined. However, the possible positions of NO_2 addition in a sequential fashion were theoretically evaluated using density functional theory simulations[21]. Among these nitrated products, the

depletion of dinitro-PBNA was found to be strongly associated with the onset of aggressive aging in NP, namely NP hydrolysis signatured by the detection of the formation of acetic/formic acids and 2,2-dinitropropanol (DNPOH). More discussion will be given for NP hydrolysis in Section 3.3.

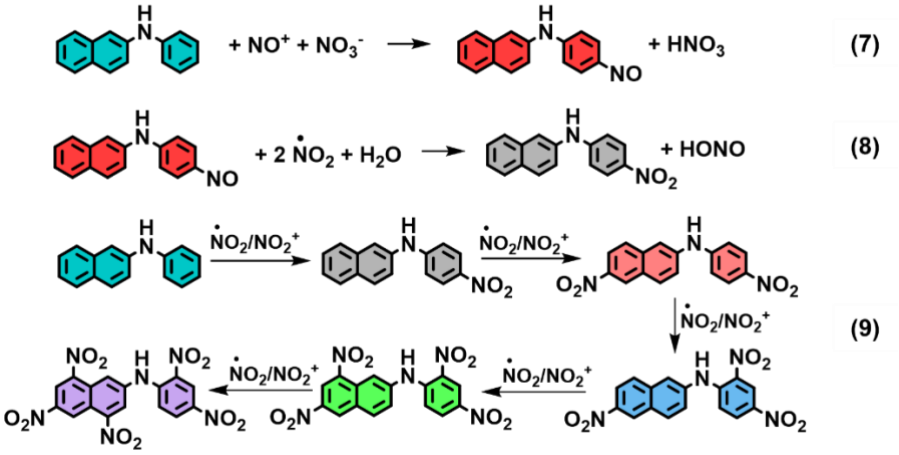

Scheme 1. Proposed PBNA reaction pathways: nitrosation (7) and the subsequent oxidation (8); and the sequential nitration (9). The PBNA-associated species are color coded to match those in the MS/MS spectra.

3.2.1 PBNA Consumption

Because all supposed baseline NP samples were produced in the 1960s, they have already been stored (more accurately, aged) for more than 55 years, the initial PBNA (0.1 wt%) was almost consumed. This residual PBNA is established as the time zero concentration in the 44-month thermal aging experiment. As expected, with higher temperature the PBNA is consumed faster than lower temperatures (**Figure 9**). Due to its poor solubility in the aqueous phase, PBNA is absent in the WW samples and the same is true for its nitroso and nitrated products as shown in **Figures 10 to 17**.

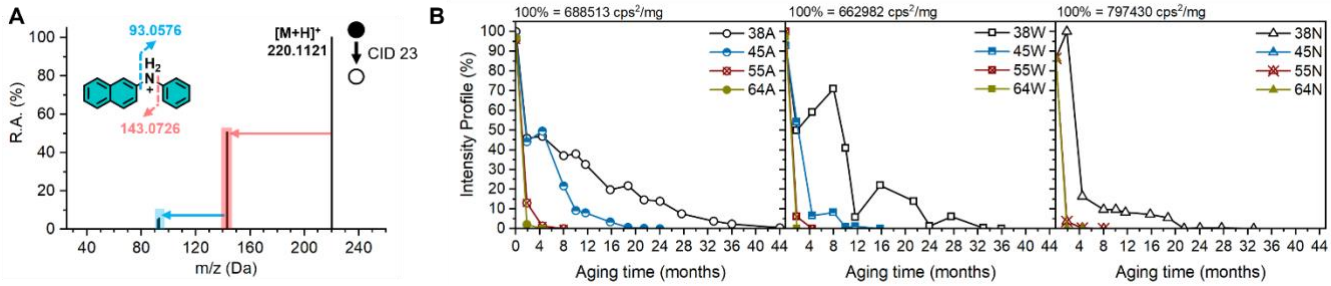

Figure 9. PBNA: MS/MS spectra showing the characteristic fragmentation in positive mode (A) and its intensity profiles in the A, W, and N samples (B).

3.2.2 Detection of Nitroso-PBNA (PBNA-NO)

Over the storage period (~55 years), most PBNA were converted into PBNA-NO via nitrosation. As aging progresses, PBNA-NO further degrades. Again, the higher the temperature the faster it is consumed.

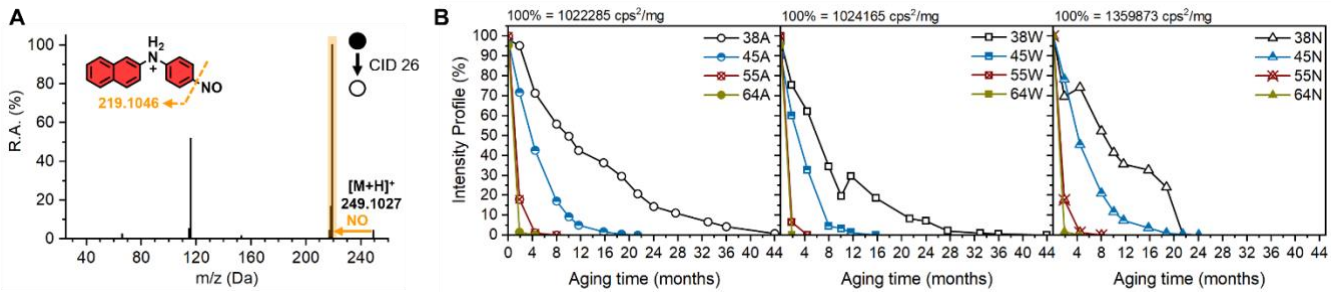

Figure 10. Nitroso-PBNA (PBNA-NO): MS/MS spectra showing the characteristic fragmentation in positive mode (A) and its intensity profiles in the A, W, and N samples (B).

3.2.3 Detection of Sequential PBNA Nitration (PBNA-xNO_2)

As the first products of sequential PBNA nitration, PBNA-NO_2 and its isomer are detected in the baseline NP (**Figures 11 and 12**). While their concentrations grow at 38 and 45°C initially and then decreases, their depletion is much more rapid at 55 and 64°C. The changes in their concentration profiles were attributed to both temperature and aging time.

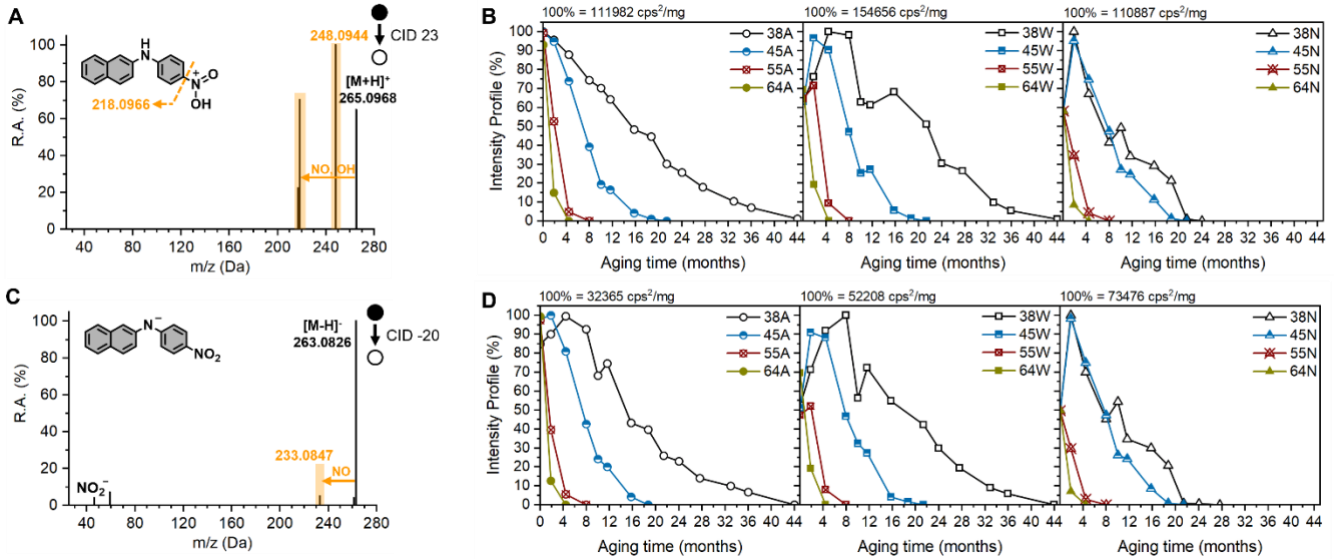

Figure 11. Mononitro-PBNA (PBNA-NO2): MS/MS spectra showing the characteristic fragmentation and its intensity profiles in A, W, and N samples in the positive (A, B) and negative (C, D) modes, respectively.

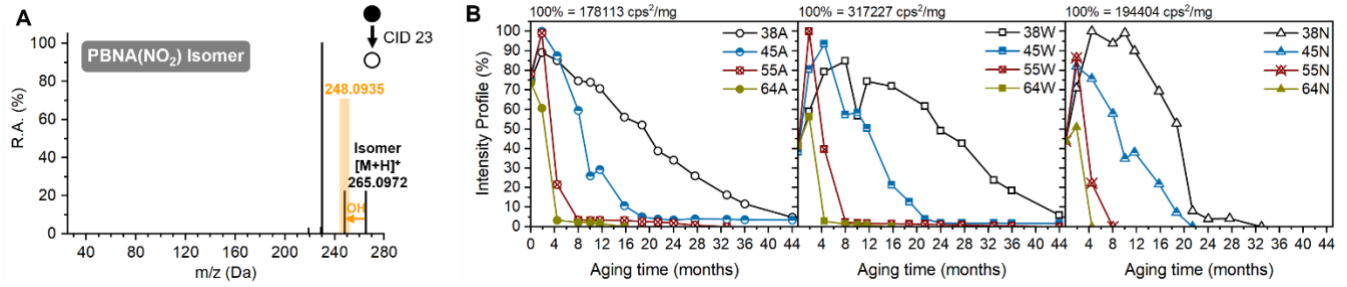

Figure 12. Mononitro-PBNA isomer: MS/MS spectra showing the characteristic fragmentation in positive mode (A) and its intensity profiles in the A, W, and N samples.

As the second products of sequential PBNA nitration, PBNA-2NO_2 and its isomer are also detected in the baseline NP (**Figures 13 and 14**), suggesting that NP degradation had progressed into the second NO_2 addition in PBNA of the baseline NP. While their concentrations gradually grow at all temperatures initially, they rapidly deplete in the order of 64°C > 55°C > 45°C > 38°C. In our recent study[21], we have demonstrated that the presence of PBNA-2NO_2 is a key indicator of NP stability. The complete depletion of PBNA-2NO_2 marks the advance of NP degradation into the late-stage where the acidity in the aged NP is sufficiently high to trigger more complicated degradation, such as acid-catalytic hydrolysis of PBNA and NP[21, 32].

As the third product of sequential PBNA nitration, PBNA-3NO_2 is not detected in the baseline NP, but it is formed as the baseline NP is continually aged (**Figure 15**). The higher the temperature, the more rapid it forms initially, but also the faster it decays. This is a typical behavior of an intermediate product in the sequential PBNA nitration process.

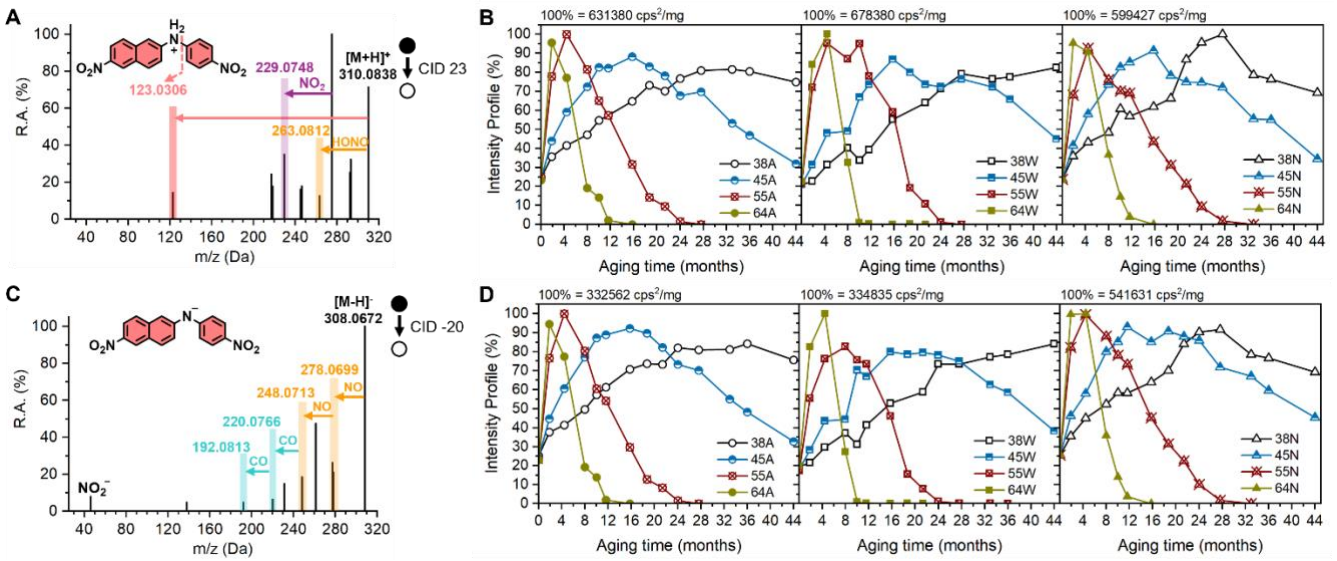

Figure 13. Dinitro-PBNA (PBNA-2NO_2): MS/MS spectra showing the characteristic fragmentation and its intensity profiles in A, W, and N samples in the positive (A, B) and negative (C, D) modes, respectively.

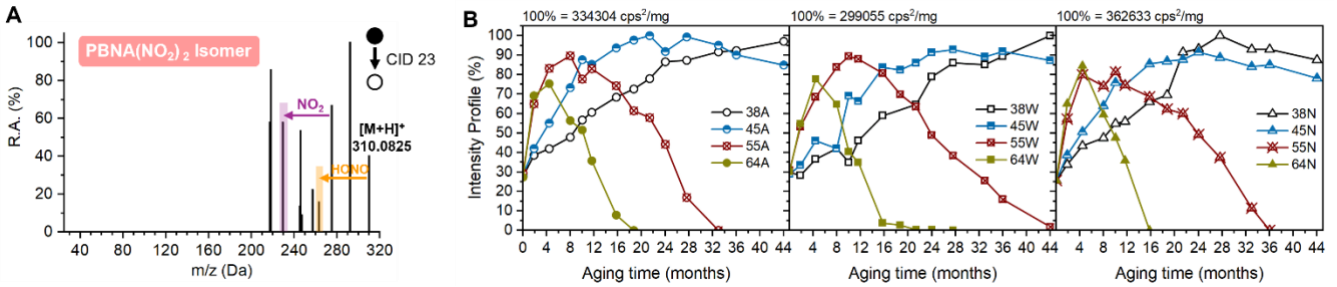

Figure 14. Dinitro-PBNA isomer: MS/MS spectra showing the characteristic fragmentation in positive mode (A) and its intensity profiles in the A, W, and N samples (B).

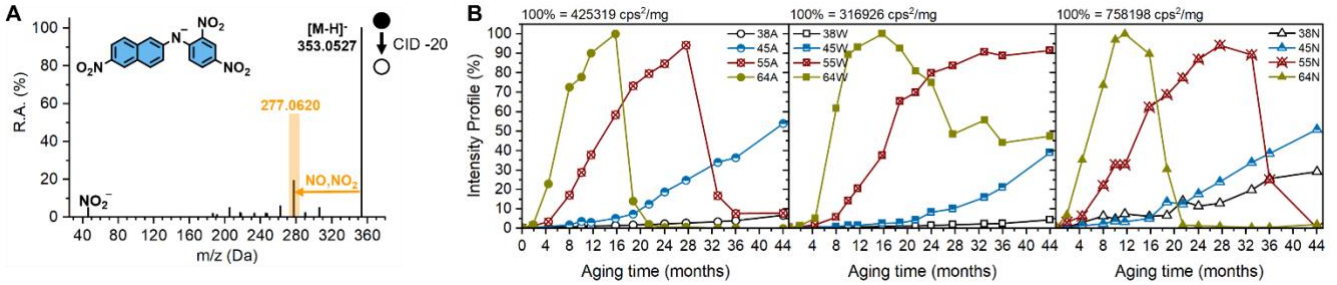

Figure 15. Trinitro-PBNA (PBNA-3NO_2): MS/MS spectra showing the characteristic fragmentation in negative mode (A) and its intensity profiles in the A, W, and N samples (B).

As expected, the late sequential PBNA nitration products, such as PBNA-4NO_2 (**Figure 16**) and PBNA-5NO_2 (**Figure 17**) are not detected in the baseline NP either. Their sole appearances in the NP samples aged at 55 and 64°C for at least a few months indicate that they are only found under aggressive aging conditions.

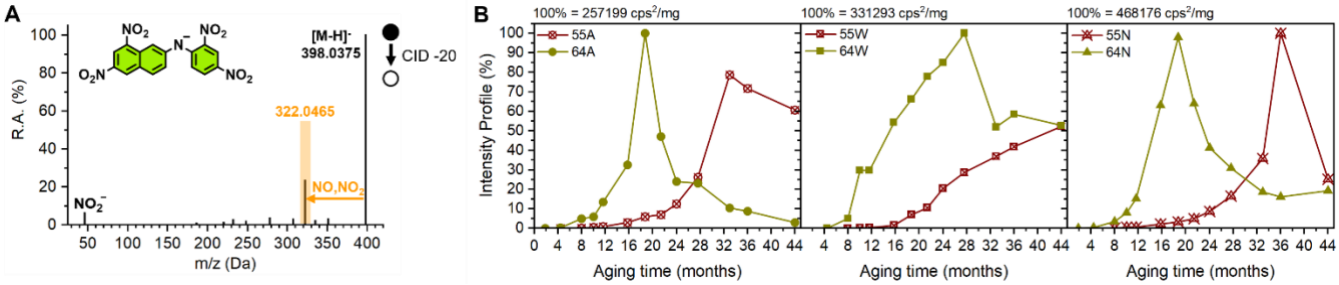

Figure 16. Tetranitro-PBNA (PBNA-4NO_2): MS/MS spectra showing the characteristic fragmentation in negative mode (A) and its intensity profiles in the A, W, and N samples (B).

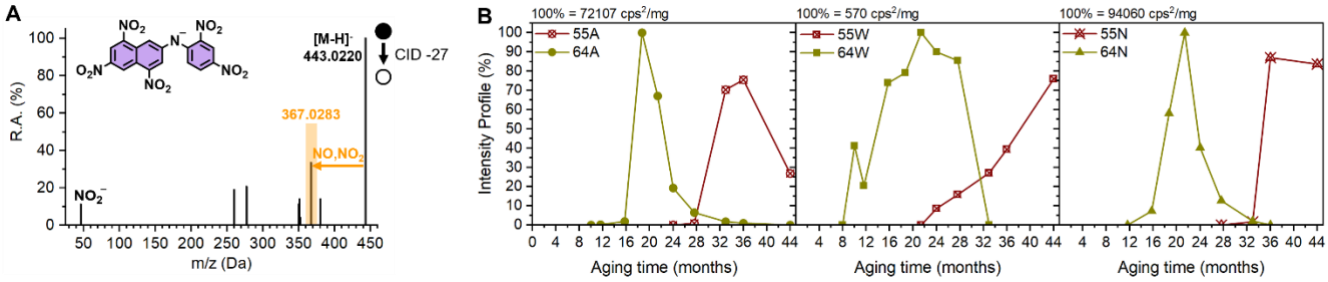

Figure 17. Pentanitro-PBNA (PBNA-5NO_2): MS/MS spectra showing the characteristic fragmentation in negative mode (A) and its intensity profiles in the A, W, and N samples (B).

3.3 Acid-catalyzed Hydrolysis and Late-stage Degradants

As shown previously in **Figures 5-17**, when aging progresses at elevated temperatures, the accumulation of water[8] and acids[22], particularly HNO_3[22, 28], increases significantly, which consumes nitroso-PBNA, PBNA-NO_2, and PBNA-2NO_2 over time. Consequently, the scavenging efficiency of PBNA decreases, resulting in more HNO_x accumulated[32], particularly in the later stage of NP degradation. Under a highly acidic environment, the protonation of NP and polynitrated PBNAs facilitates hydrolysis with water acting as the nucleophile[21], as shown in **Reactions (10), (11) and (12)** in **Scheme 2**. The hydrolysis of polynitrated PBNA is validated by the detection of nitrophenol (**Figure 18**), dinitrophenol (**Figure 19**), dinitroaniline (**Figure 20**), and dinitronaphthol (**Figure 21**)[21, 27], providing various paths of nullifying their antioxidative or anti-hydrolytic property. The prominent presence of phenol products (**Figures 18 and 19**) in the A/N samples at the elevated temperatures also verified the water generation from NP degradation in our earlier study[8], where water molecules become available for these hydrolytic reactions. Naphthoquinone (**Figure 22**) could be a byproduct of the naphthalene remnants and the reaction pathway is currently not known.

In the hydrolysis of NP, the formation of DNPOH (**Figure 23**) and acetic/formic acids in **reaction (11)** is the primary degradation route and has been quantitatively confirmed with a 2:1 (DNPOH : acetic/formic) stoichiometric ratio[22]. In the secondary degradation route, **reaction (12)**, the oxonium intermediate utilizes the decomposed NP fragments as a nucleophilic source to form various late-stage NP degradants[27]: m/z 251 (**Figure 24**), 254 (**Figure 25**), 266 (**Figure 26**), 274 (**Figure 27**), 284a (**Figure 28**), and 284b (**Figure 29**). The complexity of late-stage NP degradation is further demonstrated by the various unidentified species in **Figures 30-50**. Unique species corresponding to NP aging in air (**Figures 35-44**) versus with added water (**Figures 45-50**) were also produced, suggesting a change in the degradation pathway under different aging environment (e.g., dry vs wet); the trends of degradation (**Figures 19, 23-28**) are similar between the dry conditions i.e., N_2 and O_2. Their intensity profiles and the fragment ions are only provided as preliminary results as further investigation and enhanced MS/MS quality will be required to elucidate their structures.

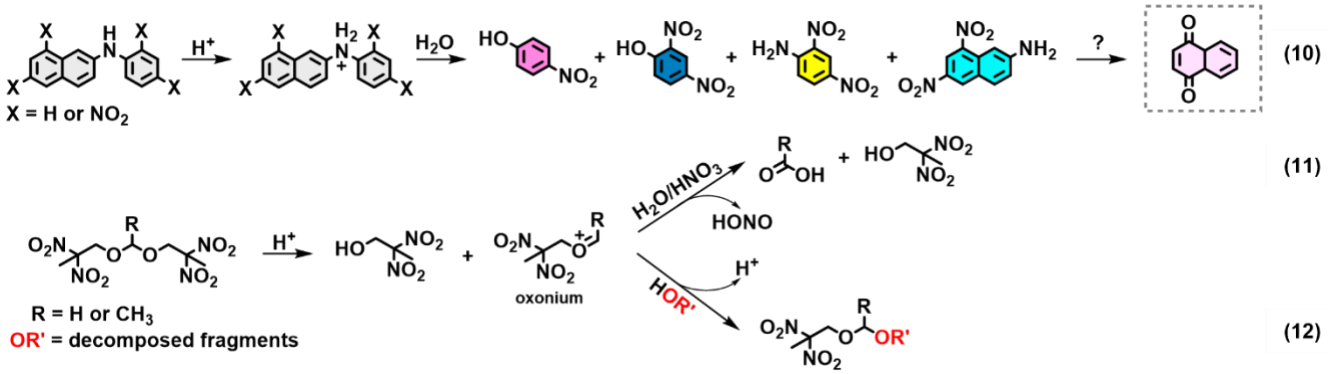

Scheme 2. Proposed reactions of acid-catalyzed hydrolysis in polynitrated PBNA (10) and NP (11); reaction between the oxonium intermediate and the decomposed NP fragments yields the late-stage NP degradants (12). The PBNA-associated species are color coded to match those in the MS/MS spectra.

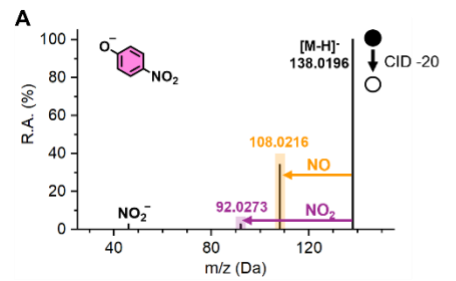

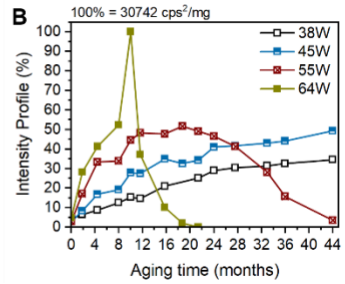

Figure 18. Nitrophenol: MS/MS spectra showing the characteristic fragmentation in negative mode (A) and its intensity profile in the W samples (B). Nitrophenol is not detected in the A/N samples, suggesting their formation prefers an environment with abundant water molecules. Similar observation is found for other species as shown in below.

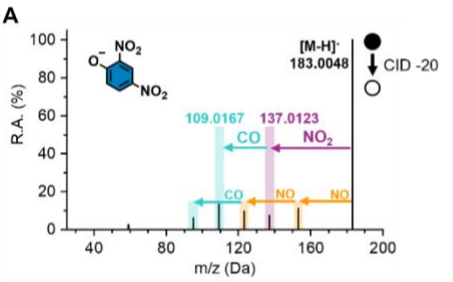

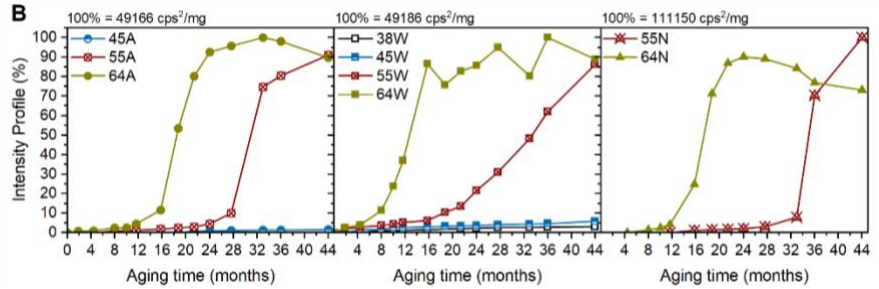

Figure 19. Dinitrophenol: MS/MS spectra showing the characteristic fragmentation in negative mode (A) and its intensity profiles in the A, W, and N samples (B). Note that water is not added in the aging process of the A and N samples, therefore the dinitrophenol detection in these samples confirms that water was generated from NP degradation. The dinitrophenol product is detected more prominently in samples aged at 55°C and above, indicating aggressive degradation condition is necessary to drive its formation. Although water molecules are readily available at the beginning of the experiment for the W samples, the abundance of dinitrophenol product is significantly lower at 45°C and below due to low acidity. Hence, both high acidity and water availability are needed for the hydrolysis of polynitrated PBNA to form the corresponding phenol products. Similar observation is found for other species as shown in below.

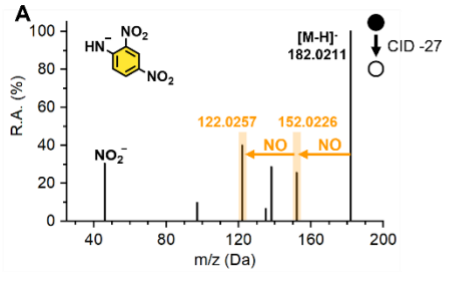

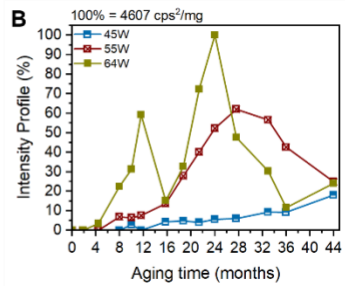

Figure 20. Dinitroaniline: MS/MS spectra showing the characteristic fragmentation in negative mode (A) and its intensity profile in the W samples (B). Dinitroaniline is not detected in the A and N samples.

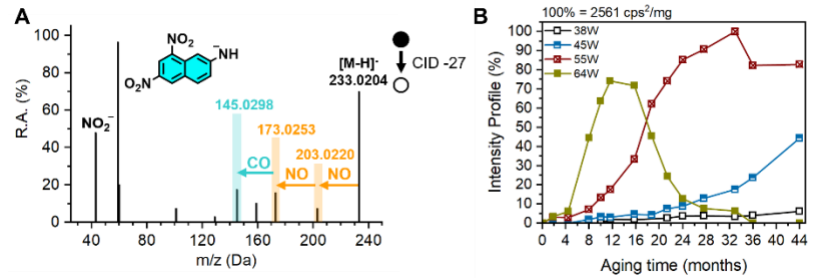

Figure 21. Dinitronaphthol: MS/MS spectra showing the characteristic fragmentation in negative mode (A) and its intensity profile in the W samples (B). Dinitronaphthol is not detected in the A and N samples.

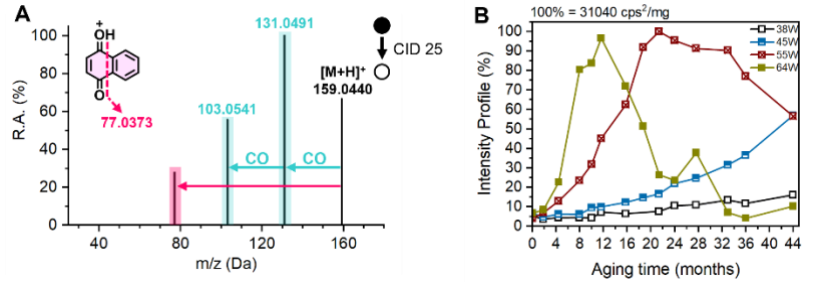

Figure 22. Naphthoquinone: MS/MS spectra showing the characteristic fragmentation in negative mode (A) and its intensity profile in the W samples (B). Naphthoquinone is not detected in the A and N samples.

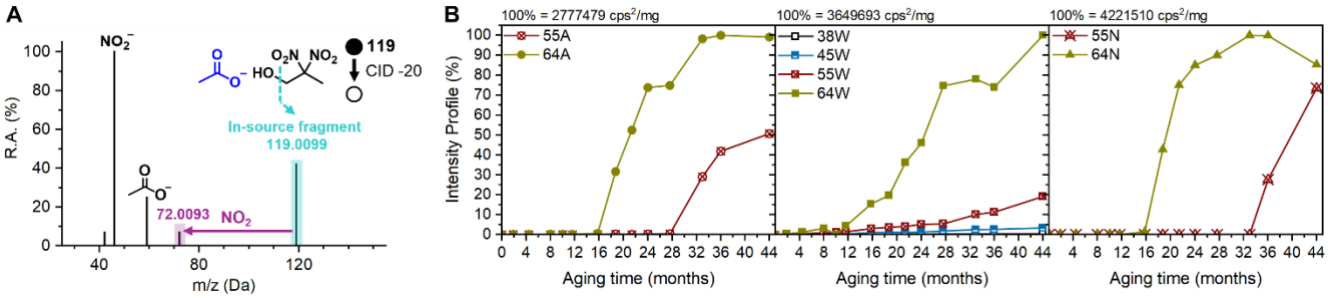

Figure 23. DNPOH: MS/MS spectra showing the characteristic fragmentation of its in-source fragment ion at m/z 119 in negative mode (A) and its intensity profile in the A, W, and N samples (B). DNPOH is not detected at low temperatures (≤45°C) in A and N samples, suggesting its formation requires a certain acidity in the aged samples. Therefore, water alone cannot drive NP hydrolysis to form DNPOH. It is the acidity which results in its formation, as indicated by their prominent presence at elevated temperatures (≥ 55°C).

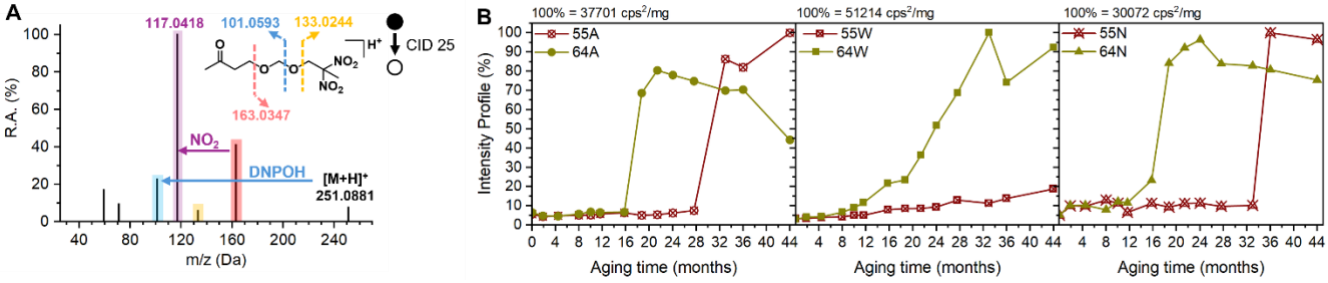

Figure 24. NP degradant at m/z 251(+): MS/MS spectra showing the characteristic fragmentation in positive mode (A) and its intensity profile in the A, W, and N samples (B). m/z 251 is only detected at elevated temperatures (≥ 55°C).

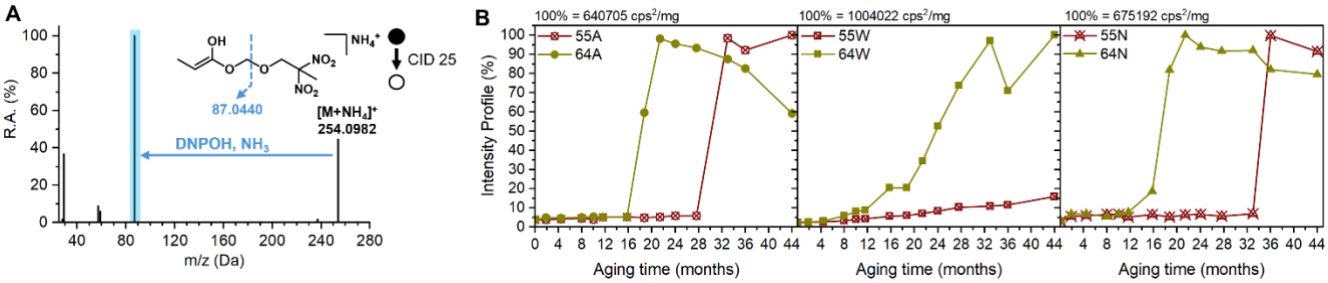

Figure 25. NP degradant at m/z 254(+): MS/MS spectra showing the characteristic fragmentation in positive mode (A) and its intensity profile in the A, W, and N samples (B). m/z 254 is only detected at elevated temperatures (≥ 55°C).

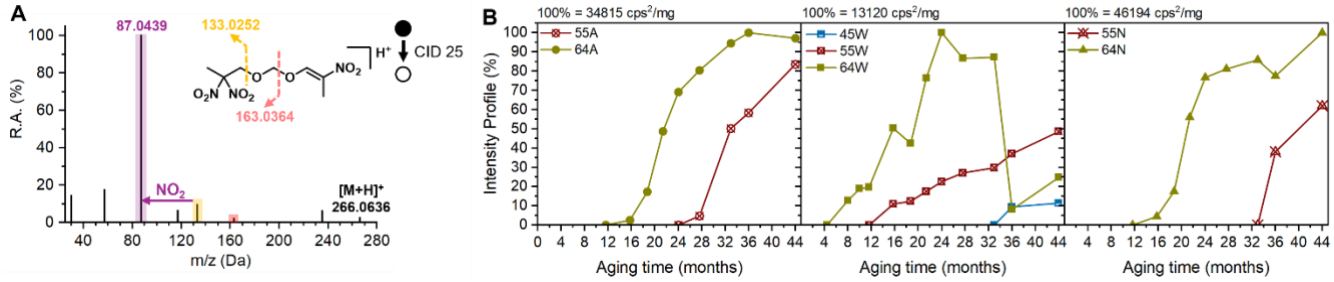

Figure 26. NP degradant at m/z 266(+): MS/MS spectra showing the characteristic fragmentation in positive mode (A) and its intensity profile in the A, W, and N samples (B). m/z 266 is only detected at ≥ 55°C of A and N samples, as well as ≥ 45°C of W samples.

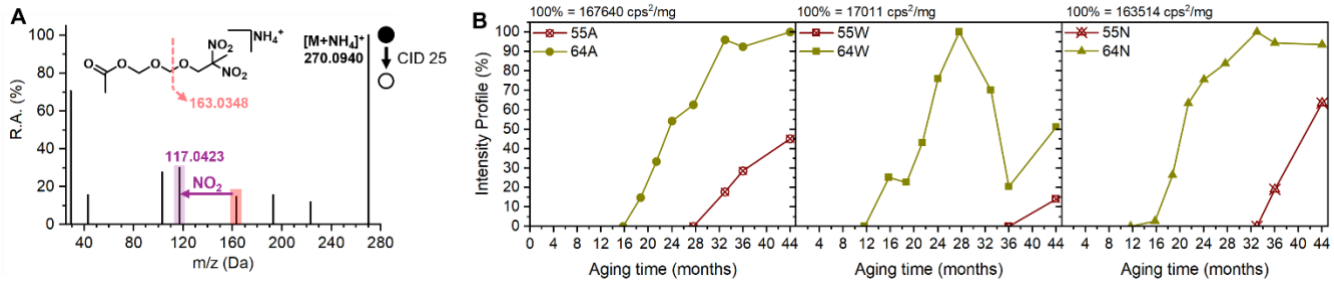

Figure 27. NP degradant at m/z 270(+): MS/MS spectra showing the characteristic fragmentation in positive mode (A) and its intensity profile in the A, W, and N samples (B). m/z 270 is only detected at ≥ 55°C.

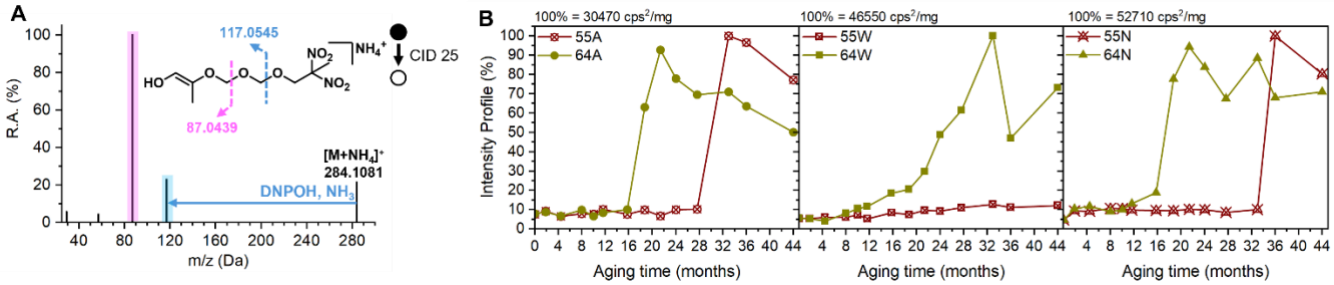

Figure 28. NP degradant at m/z 284a(+): MS/MS spectra showing the characteristic fragmentation in positive mode (A) and its intensity profile in the A, W, and N samples (B). m/z 284a is only detected at ≥ 55°C.

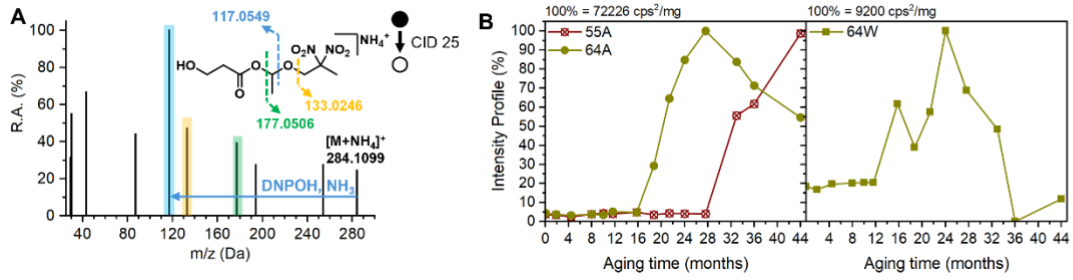

Figure 29. NP degradant at m/z 284b (+): MS/MS spectra showing the characteristic fragmentation in positive mode (A) and its intensity profile in the A, W, and N samples (B). m/z 284b is only detected at ≥ 55°C of A samples and 64°C of W samples. The data on N samples are not available.

3.4 Unidentified Species

In additional to the above identified species, there are many unidentified species also found in the LC-QTOF-MS analysis. In this section, their intensity profiles are provided to illustrate how quickly the complexity of NP degradation becomes, particularly when the aging temperatures are above 55°C. As expected, the aging environment also alters the degradation pathways. Often, the findings of these species are not as significant to the real-world applications. However, these results, along with those mentioned previously, highlight the diverse degradants generated from the complex reactions involved in the late stage of NP degradation. Therefore, the information obtained is highly dependent on the design of artificial aging experiment, such as aging temperature, aging duration, and frequency of sample collection (e.g., months, weeks, or days).

3.4.1 Detected in Air-aged and Water-aged Samples

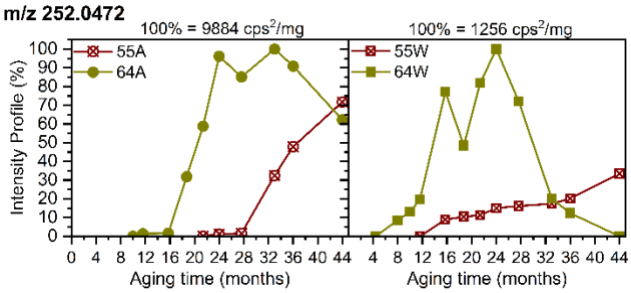

Figure 30. Intensity profile of m/z 252(-) in the A and W samples. The fragment ions of m/z 252 include m/z 119.0101, 74.9955, 59.0136, and 45.9932.

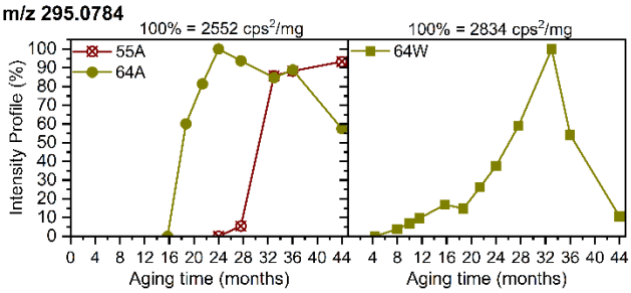

Figure 31. Intensity profile of m/z 295(-) in the A and W samples. The fragment ions of m/z 295 include m/z 102.0196, 59.01378, and 45.9933.

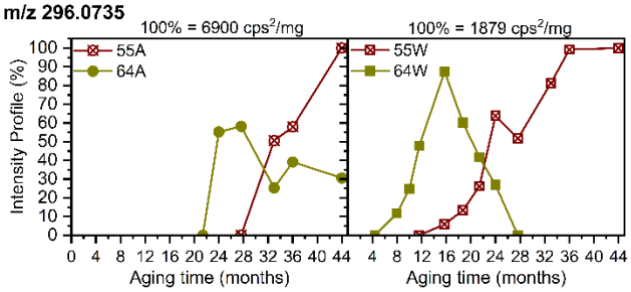

Figure 32. Intensity profile of m/z 296(-) in the A and W samples. MS/MS information is not available.

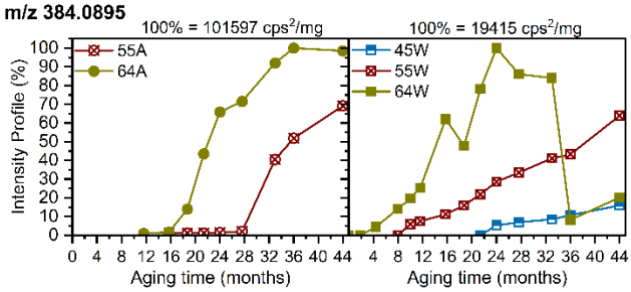

Figure 33. Intensity profile of m/z 384(-) in the A and W samples. The fragment ions of m/z 384 include 282.0579, 119.0109, 106.0132, 102.0203, 59.0137, and 45.9931.

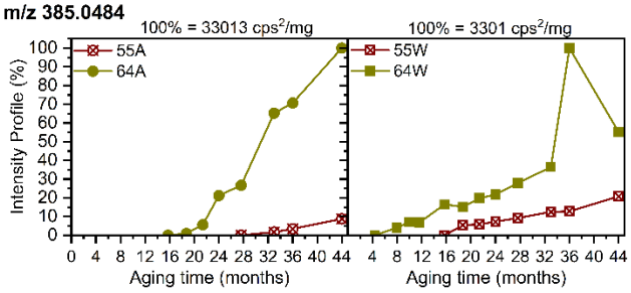

Figure 34. Intensity profile of m/z 385(-) in the A and W samples. The fragment ions of m/z 384 include 168.9894, 119.0096, 102.0199, 86.0241, 59.0134, and 45.9933.

3.4.2 Detected in Air-aged Samples Only

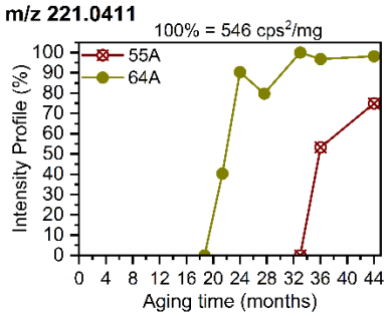

Figure 35. Intensity profile of m/z 221(-) in the A samples. MS/MS information is not available. Acetate adduct ion, m/z 281.0632, is also detected, which exhibits the same intensity profile.

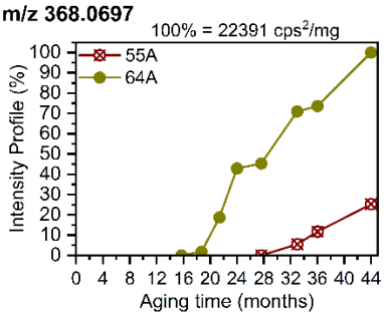

Figure 36. Intensity profile of m/z 368(-) in the A samples. The fragment ions of m/z 368 include 119.0102, 102.0200, 72.0099, and 45.9932.

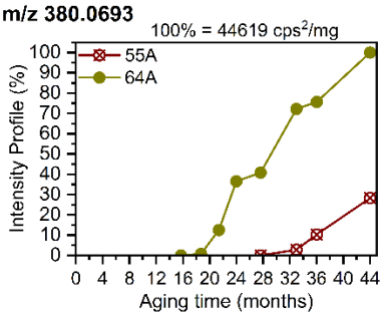

Figure 37. Intensity profile of m/z 380(-) in the A samples. The fragment ions of m/z 380 include 320.0534, 158.0206, 119.0085, 102.0200, 100.0033, 59.0138, and 45.9932.

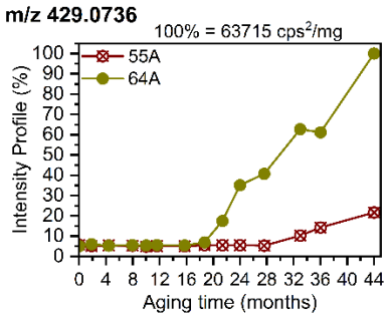

Figure 38. Intensity profile of m/z 429(-) in the A samples. The fragment ions of m/z 429 include 238.0315, 190.0354, 131.0095, 119.0098, 102.0196, 59.0137, and 45.9930.

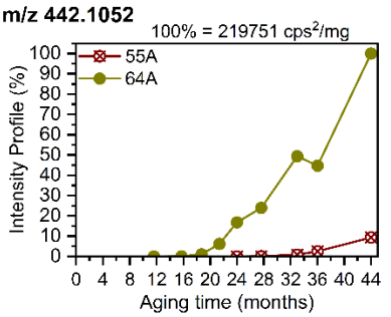

Figure 39. Intensity profile of m/z 442(-) in the A samples. The fragment ions of m/z 442 include 131.0098, 119.0093, 102.0194, 59.0136, and 45.9934.

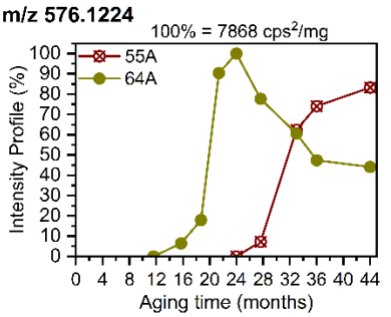

Figure 40. Intensity profile of m/z 576(-) in the A samples. The fragment ions of m/z 576 include 296.0736, 237.0361, 190.0341, 119.0101, 102.0193, and 45.9929.

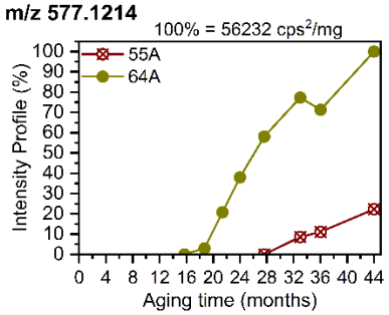

Figure 41. Intensity profile of m/z 577(-) in the A samples. The fragment ions of m/z 577 include 517.1017, 402.0729, 355.0753, 281.0364, 204.0251, 131.0097, 119.0096, 102.0194, 59.0134, and 45.9928.

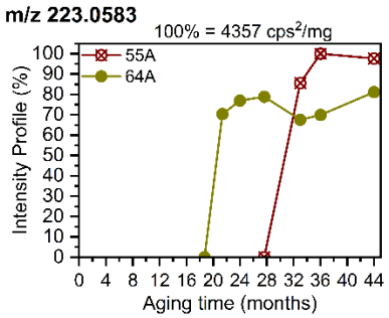

Figure 42. Intensity profile of m/z 223(+) in the A samples. The fragment ions of m/z 223 include 207.0325, 191.0002, 149.0229, 121.0280, and 73.0469.

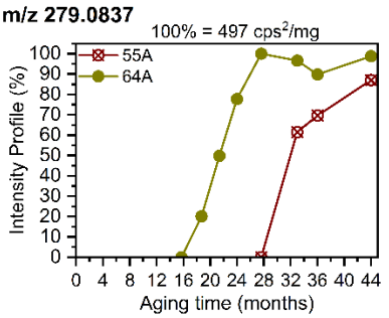

Figure 43. Intensity profile of m/z 279(+) in the A samples. The fragment ions of m/z 279 include 201.0447, 163.0358, 149.0227, and 117.0412.

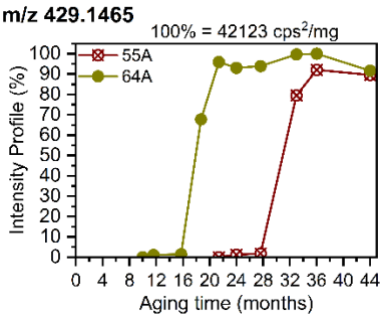

Figure 44. Intensity profile of m/z 429(+) in the A samples. The fragment ions of m/z 429 include 254.0980, 176.0557, 129.0546, and 69.0334.

3.4.3 Detected in Water-aged Samples Only

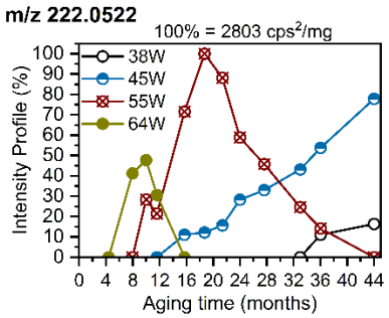

Figure 45. Intensity profile of m/z 222(-) in the W samples. The fragment ions of m/z 222 include 175.0491, 165.0289, and 45.9934.

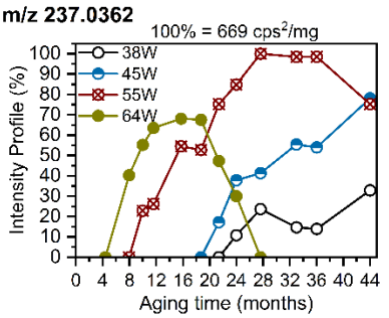

Figure 46. Intensity profile of m/z 237(-) in the W samples. The fragment ions of m/z 237 include 219.0292, 119.0140, 102.0198, 59.0129, and 45.9942.

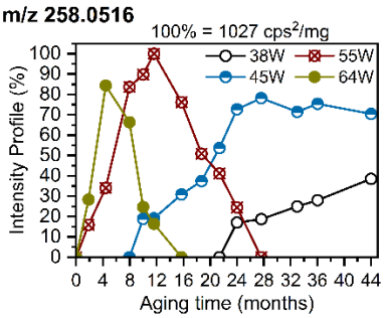

Figure 47. Intensity profile of m/z 258(-) in the W samples. The fragment ions of m/z 258 include 212.0578, 198.0560, 90.0346, and 59.0171.

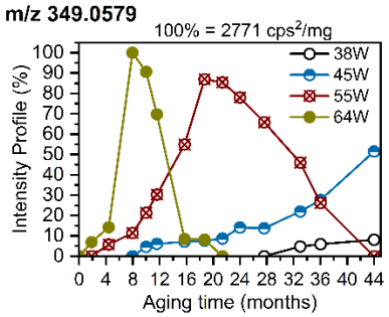

Figure 48. Intensity profile of m/z 349(-) in the W samples. The fragment ion of m/z 349 include 319.0606.

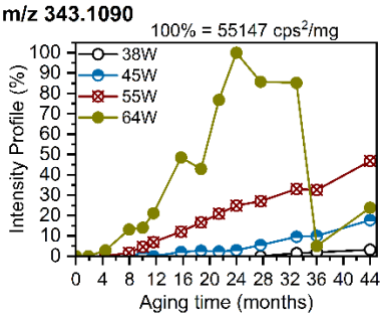

Figure 49. Intensity profile of m/z 343(+) in the W samples. m/z 343 is speculated as an ammonium adduct ion because its sodium adduct ion, m/z 348, is also detected. The fragment ions of m/z 343 include 279.0806, 266.0647, 254.0994, 235.0558, 163.0365, 117.0426, 87.0438, and 60.0446; while those of m/z 348 include 259.0544, 213.0612, 170.0423, and 125.0216.

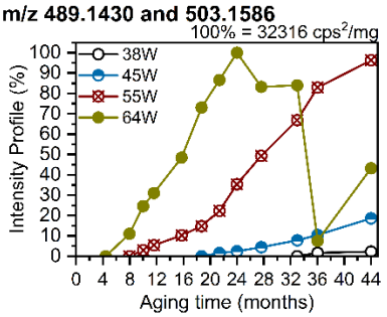

Figure 50. Unresolved intensity profile of m/z 489(+) and 503(+) in the W samples, due to similar retention times (i.e. peaks overlap at 5.0 min). The fragment ions of m/z 489 include 254.1005, 236.0539, 206.0790, 189.0511, 163.0350, 143.0585, 117.0417, and 87.0443, while those of m/z 503 include 268.1168, 263.0878, 189.0522, 177.0510, 143.0578, 133.0244, and 101.0597.

3.5 Caveats

For mechanistic investigation and chemical profiling of NP aging, choices of artificial aging conditions and characterization techniques are of paramount importance. As demonstrated by the 44-month aging experiment, the degradation species were given time for growth and decomposition due to an extended aging period at various temperatures (from RT to 64°C), which provides distinguishable trends for easier identification. Even so, information on some reaction products could still be lost without carefully and timely monitoring (e.g., frequency of sample collection). For instance, the earliest product that we discovered thus far, nitroso-PBNA, was enabled in a 21-weeks short-term experiment[28, 31]. Due to the low frequency of sample collection in the 44-month aging experiment (e.g., about every 3 months) and the additional two-year of storage in refrigeration before conducting this study, we speculate some of the short-lived intermediate species in the Chili chart[33] already disappeared and therefore not detected.

On the other hand, LC-QTOF-MS was vital for enabling the findings summarized in this library, whereas other analytical techniques do not provide such sensitivity and specificity in the vast chemical space of aged NP. However, one must approach LC-QTOF-MS experiments with extreme care as any changes in the instrumental settings could impact data quality[34]. Additionally, it is essential to follow strict analytical guidelines for accurate identification of species (e.g., retention time reproducibility of ±0.1 min and mass accuracies of ±5 ppm for precursor ion and ±10 ppm for fragment ions)[35-37]. By applying these guidelines, most of the preliminary m/z values reported in the Chili chart[33] were ejected due to high mass errors (> 20 ppm), except for m/z 296.0735, 221.0411, and 237.0362, as shown in **Figures 32, 35, and 46**. The presence of these three ions at only the elevated temperatures is consistent with proposed scheme in the Chili chart to some degree, where heat is involved for the formation of $C_4H_6N_2O_6$, $C_6H_{10}N_2O_7$, and $C_6H_{11}N_3O_7$ (i.e., predicted structures 9, 12 and 13), respectively. However, these ions cannot be structurally verified, either due to the absence of MS/MS spectra or poor MS/MS spectrometric quality, which could be caused by low ion intensity or imply that they are ion complexes. Without correction for strict cut-offs, false interpretation could arise, such as the misinterpretation of m/z 263 and 443 as impurities (**Figure 51**, left) in Pantex's evaluation[38] when they are actually mononitro-PBNA and pentanitro-PBNA (**Figure 51**, right), respectively.

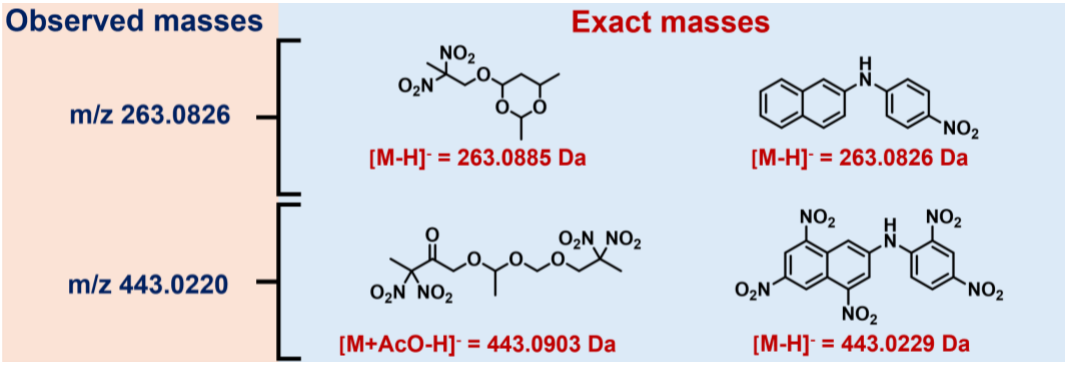

Figure 51. Observed m/z 263 and 443 (pink area) in the negative MS mode incorrectly identified as Rindone's compound V[17] and impurity (blue area, left) in Pantex 2022 evaluation[38] and correctly identified as mononitro-PBNA and pentanitro-PBNA within 5-ppm mass accuracy (blue area, right) in our studies[21, 23], respectively.

Ions with low abundance are often dismissed as insignificant fragments, which may lead to potential loss of crucial mechanistic information. This is because the ion signal strength is determined by the ionization efficiency and electrospray ionization favors polar molecules. Therefore, different techniques such as atmospheric pressure chemical ionization (APCI) may enhance their signals and/or provide access to the discovery of new species (e.g., less polar, volatile to semi-volatile compounds), online derivatization (e.g., post-column, ion-ion or ion-molecule gas-phase reactions) for targeting molecules with unique functional groups (e.g., carbonyl, phenyl, nitro), or optical-based methods (e.g., UV-vis, IR, Surface-Enhanced Raman Spectroscopy, etc.) to provide orthogonal characterization.

4. Conclusion

Based on our identification of 4 acidic species, 14 PBNA-related species, and 7 NP-related species using LC-QTOF and IC, various reaction mechanisms were proposed to unravel the complexity in the NP degradation chemistry. A comprehensive summary is provided in our recent published work[26]. The enormous chemical space and intricate aging behavior were further demonstrated by the 21 unidentified species here, which also highlighted the chemical difference between aging environments. This library is intended to provide concise and important findings to support HONO elimination as initiation of NP degradation, followed by much more complex reactions which highly depend on the aging conditions under which NP is exposed. These results are evidenced despite the absence of most species in the Chili chart. For future NP-related research, one should consider the following factors: 1) the experimental parameters to magnify the aging behavior of NP at a specific stage, e.g., early to mid-stage; 2) the type of analytical technique (e.g., APCI, derivatization, optical) to target specific class of compounds; and 3) the annotation criteria to avoid misinterpretation in the previous works which include some of ours, and the valuable findings reported here can be used as a reference. Although not emphasized in the present paper, separation of complex mixture such as aged NP samples is equally important and should be explored further (e.g., capillary electrophoresis). Additionally, the proposed impurities (**Figure 2**) in Rindone's work should be re-evaluated using modern instrumentation and with meticulous scrutiny, as the false identification of m/z 263 as "compound V" persists in numerous technical reports, whereas our work confidently identified m/z 263 as mononitro-PBNA. Finally, this study assertively demonstrates that temperature significantly accelerates NP degradation. To make NP aging is more relevant to LANL weapon system application conditions, aging temperatures should not be higher than 70°C.

Acknowledgements

We thank Justine Yang and Camille Wong for their experimental work preceding this publication, Kevin Morris (Consolidated Nuclear Security Pantex) for his parallel work of NP evaluation, Zhenghua Li and Oana Marina for the IC analysis, and Katharine Orr for helping to retrieve the LC/QTOF data. Finally, we thank Dr. Phil Leonard, although no longer with us, for sharing his valuable inputs on NP hydrolysis and PBNA nitration. This work was supported by the US Department of Energy through the Los Alamos National Laboratory Aging and Lifetimes Program. Los Alamos National Laboratory is operated by Triad National Security, LLC, for the National Nuclear Security Administration of U.S. Department of Energy (Contract No. 89233218CNA000001).

References

1. M. R. Salazar, S. L. Thompson, K. E. Laintz, T. O. Meyer and R. T. Pack, Degradation of a poly(ester urethane) elastomer. IV. Sorption and diffusion of water in PBX 9501 and its components, *J. Appl. Polym. Sci.*, 2007, **105**, 1063-1076.
2. R. A. Pesce-Rodriguez, C. S. Miser, K. L. McNesby, R. A. Fifer, S. Kessel and B. D. Strauss, Characterization of Solid Propellant and Its Connection to Aging Phenomena, *Appl. Spectrosc.*, 1992, **46**, 1143-1148.
3. D. Kumari, R. Balakshe, S. Banerjee and H. Singh, Energetic plasticizers for gun & rocket propellants, *Rev. J. Chem.*, 2012, **2**, 240-262.
4. A. Provatas, Energetic Polymers and Plasticisers for Explosive Formulations – A Review of Recent Advances, 2000, 51.
5. C. F. Melius and M. C. Piqueras, Initial Reaction Steps in the condensed-phase decomposition of propellants, *Proc. Combust. Inst.*, 2002, **Volume 29**, 2863-2871.
6. D. K. Pauler, N. J. Henson and J. D. Kress, A mechanism for the decomposition of dinitropropyl compounds, *Phys. Chem. Chem. Phys.*, 2007, **9**, 5121-5126.
7. M. R. Salazar, J. D. Kress, J. M. Lightfoot, B. G. Russel, W. A. Rodin and L. Woods, Experimental Study of the Oxidative Degradation of PBX 9501 and its Components, *Propellants Explos. Pyrotech.*, 2008, **33**, 182-202.
8. D. Yang and D. Z. Zhang, Role of water in degradation of nitroplasticizer, *Polym. Degrad. Stab.*, 2019, **170**.
9. A. Edgar, J. Yang, M. Chavez, M. Yang and D. Yang, Physical characterization of Bis(2,2-dinitropropyl) acetal and Bis(2,2-dinitropropyl) formal, *Journal of Energetic Materials*, 2020, **38**, 483-503.
10. A. S. Edgar, L. A. Goodwin, C. H. Wong and D. Yang, *Aging and Lifetimes Program FY 2022 Annual Report - Part I: Update to BDNPA-BDNPF phase diagram*, Report LA-UR-22-31516, Los Alamos National Laboratory, Los Alamos, NM 87545.
11. D. Yang, K. Chen, A. S. Edgar, I. Matanovic, J. Jung and J. D. Kress, Recent progress in aging studies of a eutectic mixture of bis(2,2-dinitropropyl) acetal and formal nitroplasticizer, *Polym. Degrad. Stab.*, 2023, **218**.

12. R. S. Booth, C. S. Lam, M. D. Brynteson, L. Wang and L. J. Butler, Elucidating the decomposition mechanism of energetic materials with geminal dinitro groups using 2-bromo-2-nitropropane photodissociation, *J Phys Chem A*, 2013, **117**, 9531-9547.
13. S. Désilets and S. Villeneuve, Trace Determination of Strong Acids in NitroPlasticizers, *The Analyst*, 1997, **122**, 995-998.
14. D. A. Wrobleski, D. A. Langlois, E. B. Orler, R. D. Gilbertson, D. M. Dattelbaum, B. J. Hornstein and J. H. Small, *Oxidative degradation chemistry of PBX 9501 binder analogs using isotopic labeling.*, Report LA-UR-04-8236, Los Alamos National Laboratory, 2004.
15. D. Yang, R. Pacheco, S. Edwards, K. Henderson, R. Wu, A. Labouriau and P. Stark, Thermal stability of a eutectic mixture of bis(2,2-dinitropropyl) acetal and formal: Part A. Degradation mechanisms in air and under nitrogen atmosphere, *Polym. Degrad. Stab.*, 2016, **129**, 380-398.
16. D. Yang, R. Pacheco, S. Edwards, J. Torres, K. Henderson, M. Sykora, P. Stark and S. Larson, Thermal stability of a eutectic mixture of bis(2,2-dinitropropyl) acetal and formal: Part B. Degradation mechanisms under water and high humidity environments, *Polym. Degrad. Stab.*, 2016, **130**, 338-347.
17. R. Rindone, D. A. Geiss and H. Miyoshi, IM/EM Technology Implementation in the 21st Century: BDNPA/BDNPF shows long-time aging stability.*Journal*, 2000.
18. C. H. Wong, A. S. Edgar and D. Yang, Liquid Chromatography Mass Spectrometry Study of a Eutectic Mixture of bis(2,2-Dinitropropyl) Acetal/Formal, *Propellants Explos. Pyrotech.*, 2021, **46**, 1849-1859.
19. D. Yang, A. S. Edgar, J. A. Torres, J. C. Adams and J. D. Kress, Thermal Stability of a Eutectic Mixture of Bis(2,2-dinitropropyl) Acetal and Formal: Part C. Kinetic Compensation Effect, *Propellants Explos. Pyrotech.*, 2020, **46**, 134-149.
20. A. S. Edgar, C. H. Wong, K. Chen, D. A. Langlois and D. Yang, Identification of 2,2-dinitropropanol, a Hydrolyzed Product of Aged Eutectic Bis(2,2-dinitropropyl) Acetal – Bis(2,2-dinitropropyl) Formal Mixture, *Propellants, Explosives, Pyrotechnics*, 2022, **47**.
21. K. Chen, A. S. Edgar, J. Jung, J. D. Kress, C. H. Wong and D. Yang, Liquid Chromatography Quadrupole Time-of-Flight Mass Spectrometry Analysis of Eutectic Bis(2,2-dinitropropyl) Acetal/Formal Degradation Profile: Nontargeted Identification of Antioxidant Derivatives, *ACS Omega*, 2022, **7**, 35316-35325.
22. K. Chen, A. S. Edgar, Z. H. Li, O. C. Marina and D. Yang, Roles of HNOx and Carboxylic Acids in the Thermal Stability of Nitroplasticizer, *ACS Omega*, 2023, **8**, 14730-14741.
23. K. Chen, A. S. Edgar, C. H. Wong and D. Yang, Liquid Chromatography Quadrupole Time-of-Flight Mass Spectrometry: A Strategy for Optimization, Characterization, and Quantification of Antioxidant Nitro Derivatives, *ACS Omega*, 2022, **7**, 32701-32707.
24. K. Chen, J. D. Kress and D. Yang, New insight: Nitrosation of n-phenyl-β-naphthylamine in the early stage of nitroplasticizer aging, *Polymer Degradation and Stability*, 2023, **217**, 110541.
25. K. Chen and D. Yang, *Fast Semi-automated Postprocessing Workflow of Untargeted LC-QTOF-MS Data for Aging Study*, Report LA-UR-23-20482, Los Alamos National Laboratory, Los Alamos, NM 87545, 2023.
26. D. Yang, K. Chen, A. S. Edgar, I. Matanovic, J. Jung and J. D. Kress, Recent progress in aging studies of a eutectic mixture of bis(2,2-dinitropropyl) acetal and formal nitroplasticizer, *Polymer Degradation and Stability*, 2023, **218**, 110565.
27. K. Chen, A. S. Edgar and D. Yang, *Tandem MS Elucidation of Late-Stage Degradation Mechanism of Nitroplasticizer*, Report LA-UR-24-25037, Los Alamos National Laboratory, Los Alamos, NM 87545, 2024.
28. K. Chen, J. D. Kress, D. Yang, A. S. Edgar, O. C. Marina, Z. Li and J. K. Brett, *Role of n-phenyl-β-naphthylamine in the Acid-Nitroplasticizer Thermal Aging (ANTA) Experiment*, Report LA-UR-23-32645, Los Alamos National Laboratory, Los Alamos, NM 87545, 2023.
29. P. Y. Bruice, in *Organic Chemistry*, Pearson Prentice Hall, Upper Saddle River, NJ, 5th edn., 2007, pp. 704-706.
30. D. L. H. Williams, The mechanism of the Fischer-Hepp rearrangement of aromatic N-nitroso-amines, *Tetrahedron*, 1975, **31**, 1343-1349.
31. K. Chen, J. D. Kress and D. Yang, New insight: Nitrosation of n-phenyl-β-naphthylamine in the early stage of nitroplasticizer aging, *Polym. Degrad. Stab.*, 2023, **217**.
32. K. Chen, A. S. Edgar, Z. H. Li, O. C. Marina and D. Yang, Roles of HNO (x) and Carboxylic Acids in the Thermal Stability of Nitroplasticizer, *ACS Omega*, 2023, **8**, 14730-14741.
33. C. H. Wong, A. S. Edgar and D. Yang, *Characterization of Artificially Aged Nitroplasticizer: Liquid Chromatography Tandem Quadrupole Time of Flight Mass Spectrometry Identified Signals of Reactants, Intermediates, and Degradation Products*, Report LA-UR-21-28681, Los Alamos National Laboratory, Los Alamos, NM 87545, 2021.
34. E. Defossez, J. Bourquin, S. von Reuss, S. Rasmann and G. Glauser, Eight key rules for successful data-dependent acquisition in mass spectrometry-based metabolomics, *Mass Spectrom Rev*, 2023, **42**, 131-143.
35. 2002/657/EC: Commission Decision of 12 August 2002 implementing Council Directive 96/23/EC concerning the performance of analytical methods and the interpretation of results.*Journal*, 2002.
36. European Commision, Analytical Quality Control and Method Validation Procedures For Pesticide Residues Analysis in Food and Feed SANTE/11312/2021, 2021.
37. H. Oberacher, M. Sasse, J.-P. Antignac, Y. Guitton, L. Debrauwer, E. L. Jamin, T. Schulze, M. Krauss, A. Covaci, N. Caballero-Casero, K. Rousseau, A. Damont, F. Fenaille, M. Lamoree and E. L. Schymanski, A European proposal for quality control and quality assurance of tandem mass spectral libraries, *Environmental Sciences Europe*, 2020, **32**, 43.
38. K. D. Morris, *Aged Nitroplasticizer Evaluation*, Report PXRPT 22-01, CNS, LLC., Pantex Plant, Amarillo, TX, USA, 2022.